Author/s:
Molakarimi, M;Gorman, MA;Mohseni, A;Pashandi, Z;Taghdir, M;Naderi-Manesh, H;Sajedi, RH;Parker, MW

Title:
Reaction mechanism of the bioluminescent protein mnemiopsin1 revealed by X-ray crystallography and QM/MM simulations

Date:
2019-01-04

Citation:
Molakarimi, M., Gorman, M. A., Mohseni, A., Pashandi, Z., Taghdir, M., Naderi-Manesh, H., Sajedi, R. H. & Parker, M. W. (2019). Reaction mechanism of the bioluminescent protein mnemiopsin1 revealed by X-ray crystallography and QM/MM simulations. Journal of Biological Chemistry, 294 (1), pp.20-27. https://doi.org/10.1074/jbc.RA118.006053.

Persistent Link:
https://hdl.handle.net/11343/290306

Reaction mechanism of the bioluminescent protein mnemiopsin1 revealed by X-ray crystallography and QM/MM simulations

Received for publication, September 28, 2018, and in revised form, November 5, 2018 Published, Papers in Press, November 12, 2018, DOI 10.1074/jbc.RA118.006053

Maryam Molakarimi[‡1], Michael A. Gorman[§¶1], Ammar Mohseni[‡], Zaiddodine Pashandi[‖], Majid Taghdir[‖], Hossein Naderi-Manesh[‖], Reza H. Sajedi[‡2], and Michael W. Parker[§¶3]

From the [‡]Department of Biochemistry, Faculty of Biological Sciences, Tarbiat Modares University, Tehran 14115-154, Iran, the [‖]Department of Biophysics, Faculty of Biological Sciences, Tarbiat Modares University, Tehran 14115-175, Iran, the [§]Department of Biochemistry and Molecular Biology, Bio21 Molecular Science and Biotechnology Institute, University of Melbourne, Victoria 3010, Australia, and the [¶]Australian Cancer Research Foundation Rational Drug Discovery Centre, St. Vincent's Institute of Medical Research, Fitzroy, Victoria 3065, Australia

Edited by Karen G. Fleming

Bioluminescence of a variety of marine organisms, mostly cnidarians and ctenophores, is carried out by Ca^{2+}-dependent photoproteins. The mechanism of light emission operates via the same reaction in both animal families. Despite numerous studies on the ctenophore photoprotein family, the detailed catalytic mechanism and arrangement of amino acid residues surrounding the chromophore in this family are a mystery. Here, we report the crystal structure of Cd^{2+}-loaded apo-mnemiopsin1, a member of the ctenophore family, at 2.15 Å resolution and used quantum mechanics/molecular mechanics (QM/MM) to investigate its reaction mechanism. The simulations suggested that an Asp-156–Arg-39–Tyr-202 triad creates a hydrogen-bonded network to facilitate the transfer of a proton from the 2-hydroperoxy group of the chromophore coelenterazine to bulk solvent. We identified a water molecule in the coelenteramide-binding cavity that forms a hydrogen bond with the amide nitrogen atom of coelenteramide, which, in turn, is hydrogen-bonded via another water molecule to Tyr-131. This observation supports the hypothesis that the function of the coelenteramide-bound water molecule is to catalyze the 2-hydroperoxycoelenterazine decarboxylation reaction by protonation of a dioxetanone anion, thereby triggering the bioluminescence reaction in the ctenophore photoprotein family.

This work was supported by the Research Council of Tarbiat Modares University. This work was also supported with funding from the Victorian Government Operational Infrastructure Support Scheme to St. Vincent's Institute. The authors declare that they have no conflicts of interest with the contents of this article.

This article contains Figs. S1 and S2.

The atomic coordinates and structure factors (code 5VP3) have been deposited in the Protein Data Bank (http://wwpdb.org/).

[1] Both authors contributed equally to this work.

[2] To whom correspondence may be addressed: Dept. of Biochemistry, Faculty of Biological Sciences, Tarbiat Modares University, Tehran 14115-154, Iran. E-mail: Sajedi_R@modares.ac.ir.

[3] Recipient of National Health and Medical Research Council of Australia Research Fellowship 1117183. To whom correspondence may be addressed: Dept. of Biochemistry and Molecular Biology, Bio21 Molecular Science and Biotechnology Institute, University of Melbourne, Victoria 3010, Australia. Tel.: 61-3-9231-2499; E-mail: mparker@svi.edu.au.

Ca^{2+}-binding photoproteins are considered as valuable biological tools in a variety of biochemical fields such as gene expression analysis (1–3), drug discovery (4, 5), and protein dynamics investigations (6). These proteins consist of an apoprotein and a noncovalently bound chromophore, called peroxy-coelenterazine, located in a hydrophobic cavity. Ca^{2+} binding causes an intermolecular reaction where peroxy-coelenterazine is oxidized to coelenteramide, resulting in CO_2 release and light emission (7–9). To regenerate the active complex, the coelenteramide dissociates from the active site, together with the loss of calcium ions, to form the apoprotein. The charged photoprotein is then regenerated by the addition of peroxy-coelenterazine in the presence of molecular oxygen and the binding of calcium ions to the protein.

Structural investigations of a number of cnidarian photoproteins including aequorin, obelin, and clytin in apo (10), coelenterazine-bound (11–13), and coelenteramide-bound (14–17) states indicate that some intermediates are engaged in the oxidative decarboxylation of coelenterazine. Regeneration of the peroxy anion occurs in the presence of Ca^{2+} and with the help of a His–Tyr–Trp catalytic triad. In this mechanism, the binding of Ca^{2+} causes a conformational change that makes the hydrogen bond between His-175 and Tyr-190 (obelin numbering) stronger. As a result, His-175 and Tyr-190 residues become protonated and nucleophilic, respectively, with the tyrosine being protonated by the hydroperoxy group of coelenterazine leading to the production of a peroxy anion (8).

The only published crystal structures of a photoprotein from the ctenophore family is apo-berovin, bound to calcium (18) and magnesium ions (19). Despite the similar bioluminescence reaction and a high degree of structural similarity between the cnidarian and ctenophore photoproteins, there is a low degree of sequence identity between these families; for instance, the sequence identity between berovin and aequorin is 29.4%. Indeed, attempts to identify the catalytic triad in the cnidarian family based on structural and mutagenesis studies of the ctenophore family have not successful (18, 20–24). In our recent QM/MM study on the holo-berovin, we proposed that Asp-158–Arg-41–Tyr-204 could form a hydrogen-bonded network

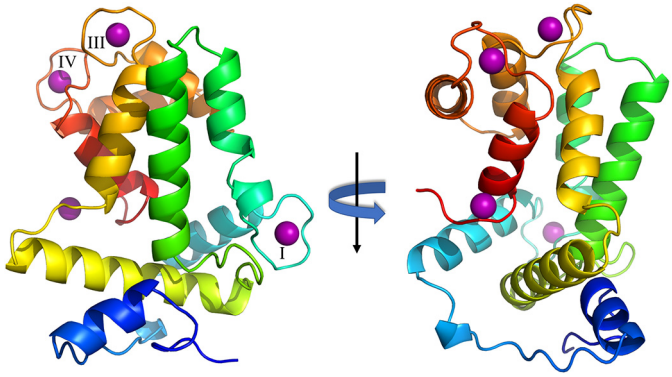

Figure 1. Cadmium ions occupy the EF-hands. A cartoon representation showing orthogonal views of mnemiopsin1 is shown. Proteins are colored from the N terminus (*blue*) to C terminus (*red*). Bound cadmium ions are shown as *purple spheres*.

around the peroxy group that could shuttle a proton from the peroxide group to bulk solvent (25).

The ctenophore family member mnemiopsin1 was originally isolated from luminous *Mnemiopsis leidyi* from the Caspian Sea in Iran and has been well-studied since (20–22, 24–27). In the present study, we report the crystal structure of apo-mnemiopsin1 at 2.15 Å resolution. The structure reveals that mnemiopsin1 has a two-domain fold with four α-helices in each domain. We then applied QM/MM[4] calculations on the structure to identify the catalytic triad of residues in the cnidarian family and to gain a detailed understanding of the reaction mechanism.

Results

Overall structure

Like other photoproteins, apo-mnemiopsin1 has a two-domain fold with four α-helices A–D and E–H in the N- and C-terminal domains, respectively (Fig. 1). The 78% sequence identity between mnemiopsin1 and berovin is reflected in the RMSD of 0.8 Å over 179 Cα atoms. Similar to apo-berovin, the C-terminal residues (residues 194–206) of apo-mnemiopsin1 are not observed in the electron density map and are assumed to be disordered. However, the N-terminal loop (residues 27–35), missing in apo-berovin, is present in the electron density map of apo-mnemiopsin1 (Fig. S1). The EF-hand interhelical hydrogen-bond network for apo-mnemiopsin1 is shown in Fig. 2. The loops of EF-hand I are paired with EF-hand II by main-chain/main-chain hydrogen bonds between Met-51 and Leu-96, Met-53 and Asp-91, and Gly-49 and Arg-98. Side-chain/side-chain hydrogen bonds occur between Asp-41 and Arg-98. The loops of EF-hand III and IV interact with each other through hydrogen bonds between main-chain atoms of Val-143 with Leu-177. Side-chain/main-chain hydrogen bonds occur between Arg-179 and Asn-129, Try-132, and Leu-177/Arg-179. Finally, side-chain/side-chain interactions are found between Asp-133 and Arg-179, Lys-176 and Thr-142/Asp-140, and Tyr-163 and Lys-149. The hydrogen bonds from Arg-35 to Lys-188 and Glu-192 together with hydrogen bonds from Arg-39 to Phe-189 cap the hydroperoxycoelenterazine cavity, resulting in a solvent-inaccessible environment.

Calcium-binding loops

The presence of three Cd^{2+} loaded EF-hand Ca^{2+}-binding loops is observed in the apo-mnemiopsin1 structure (Fig. 3). Each loop (I, III, and IV) displays a canonic pentagonal bipyramidal bound cadmium ion which is coordinated by seven oxygen atoms. The cadmium ion located at loop I is coordinated equatorially to Asp-48, Asp-46, Glu-55, and main-chain carbonyl of Lys-50. Axial coordination is achieved by Asp-44 and a water molecule. Loop III equatorial coordination of Cd^{2+} occurs via the main-chain carbonyls of Thr-142, Asp-140 and Glu-147. Axial interactions are via a water molecule and Asp-138. For loop IV, equatorial coordination to the metal occurs via Asp-170, Thr-174, Glu-178, and Glu-181. The side chain of Asp-172 and the main-chain carbonyl of Lys-176 provide the axial coordination. The average distance between the cadmium and the pairing oxygen atoms are 2.38 Å for site I, 2.46 Å for site III, and 2.53 Å for site IV. These distances are similar to EF-hands bound to Ca^{2+} ions rather than Mg^{2+} ions (19, 28). Like other Ca^{2+}-binding photoproteins, EF-hand II is not capable of binding divalent metal ions. A fourth nonfunctional cadmium ion is located between symmetry-related molecules, probably aiding crystallization.

QM/MM studies on the coelenterazine bound mnemiopsin1

To gain insights into how mnemiopsin1 binds coelenterazine, a complete model was calculated by adding residues 194–206 that were not observed in the electron density map of apo-mnemiopsin1. The missing residues were added using the mitrocomin (PDB code 4NQG) and berovin (PDB code 5BPJ) structures as templates by the I-Tasser server. The best model with C-score of −1.35, TM score of 0.55 ± 0.15, and RMSD of 8.4 ± 4.5 Å was refined by molecular dynamics (MD) simulation.

The binding orientation of coelenterazine in mnemiopsin1 was predicted by molecular docking using AutoDock (29–32). The results showed that coelenterazine docks into the mnemiopsin1 and berovin structures with a similar binding mode. To investigate the dynamic stability of the resultant docked structure, a 30-ns MD simulation was performed. The RMSD was monitored for backbone Cα atoms of mnemiopsin1 relative to the starting structure during the whole MD run (Fig. 4). The backbone trajectories of the structure were stable, reaching equilibrium after the first 10 ns of the simulation. The final model was used for subsequent computational analyses. A comparison of the holo-mnemiopsin1 and holo-berovin structures reveals identical amino acid residues in the binding cavity. Asn-105, Lys-88, and Trp-101 residues interact with the oxygen of the 6-ρ-hydroxybenzyl group of coelenterazine. The hydroxyl group of Tyr-202 has a predicted strong hydrogen bond to the 2-hydroperoxy group of coelenterazine. Arg-39, Asp-156, and Trp-190 residues were also observed close to the 2-hydroperoxy group. Furthermore, the 2-ρ-hydroxybenzyl group of coelenterazine is stabilized through hydrogen bonding with Ser-128 side chain.

[4] The abbreviations used are: QM/MM, quantum mechanics/molecular mechanics; MD, molecular dynamics; RMSD, root-mean-squared deviation; PDB, Protein Data Bank.

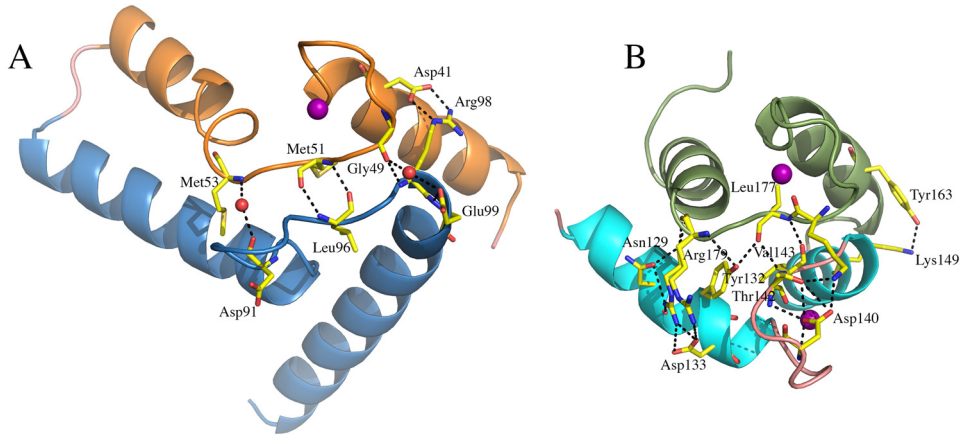

Figure 2. Hydrogen-bond interactions in EF-hands. *A*, between loops of EF-hand I and I. *B*, between loops of EF-hand III and IV.

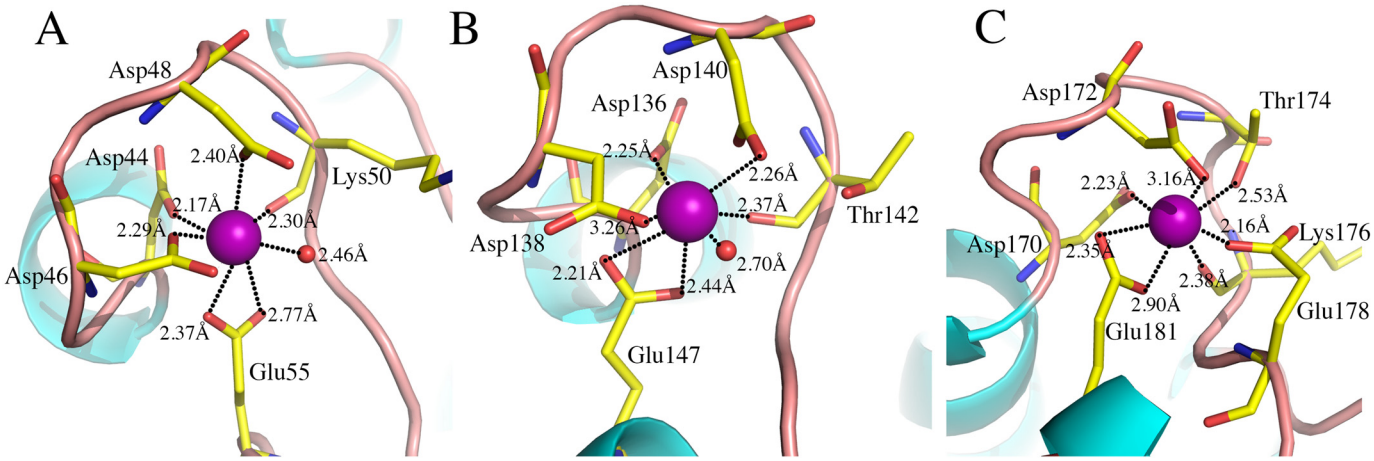

Figure 3. Cartoon representation showing the bond coordination for EF-hand I (*A*), III (*B*), and IV (*C*). Water and cadmium ions are shown as *red* and *purple spheres*, respectively.

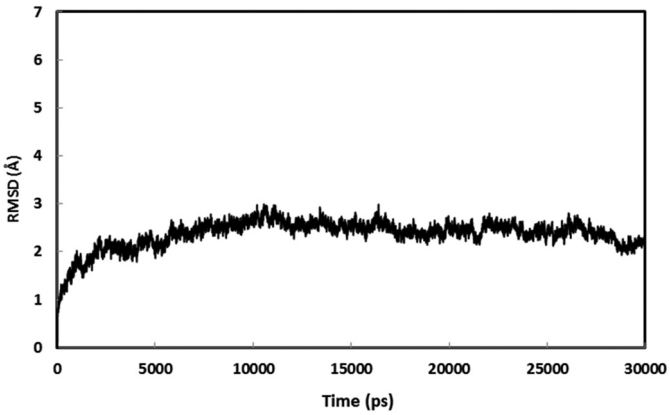

Figure 4. MD simulation of the coelenterazine bound mnemiopsin1. The graph shows the RMSD of the backbone Cα atoms of the mnemiopsin1 with respect to the first snapshot during the simulation as a function of time.

QM/MM calculations on mnemiopsin1 were performed similar to that described in the recent study on berovin (25). In the previous study, we only observed the presence of Asp-158–Arg-41–Tyr-204 triad around the 2-hydroperoxy group (25). As shown in Fig. 5, additional insight comes from consideration of the QM/MM calculations on the mnemiopsin1 structure in which transfer of a proton from the hydroperoxide group of coelenterazine to Tyr-202 is observed. A nucleophilic attack of the peroxy anion of coelenterazine onto its C_3 position results in a dioxetane intermediate, so that the distance of C_3–O_{34} decreases from 3.64 to 1.57 Å, whereas the distance of N_4–C_3 is increased from 1.41 to 1.55 Å (Table 1).

QM/MM studies on the coelenteramide-bound mnemiopsin1

The coelenteramide was oriented into the mnemiopsin1 structure in the same orientation as we previously docked coelenterazine. The resultant complex was refined by MD simulation and used for QM/MM analyses. The hydroxyl group of Tyr-131 is 7.5 Å from N1 of 2-hydroperoxycoelenterazine. In addition, in the apo-mnemiopsin1 structure the Tyr-131 hydroxyl group forms a hydrogen bond to a water molecule (Fig. S2), both of which are far from the N1 atom (Fig. 6*A*). Based on the bioluminescence mechanism in the cnidarian family, the amide anion would be protonated before it has a chance for radiative emission. Thus, in the QM/MM calculations of Ca^{2+}-discharged mnemiopsin1, this water molecule was manually protonated to form a hydronium ion. In an optimized structure, this water molecule forms a strong hydrogen bond with the amide N atom of coelenteramide (Fig. 6*B*). As shown in Fig. 6*C*, at the end of calculations, the proton was

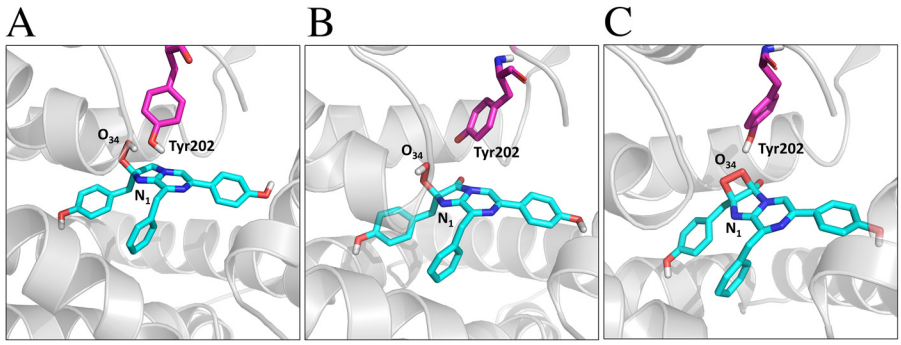

Figure 5. Close-up views of the coelenterazine-binding site in the mnemiopsin1 model. *A*, from the last snapshot of the MD simulation. *B*, from the step that the Tyr-202 was manually deprotonated to form a tyrosinate anion. *C*, from the last snapshot of the QM/MM. The proton is transferred from water molecule to N1 atom, and the dioxetane intermediate is formed.

Table 1
Selected bond lengths (Å) of coelenterazine obtained from the MD simulation and QM/MM studies

Selected bonds	MD simulation	QM/MM simulation
O34–C3	3.64	1.57
N4–C3	1.41	1.55

transferred from of water molecule to the amide N atom of coelenteramide.

Discussion

The structure of mnemiopsin1 bound to cadmium ions reveals a similar topology to that of berovin complexed with calcium (18) and magnesium ions (19). Based on the structure of aequorin bound to coelenterazine, the proposed substrate-binding site of mnemiopsin1 is located in the core of the protein, surrounded by four EF-hand loops that provide a fairly hydrophobic pocket that contains mostly hydrophobic side chains but some hydrophilic aromatic residues.

The bioluminescence reaction in both photoprotein families of cnidarians and ctenophores appear to be similar. However, the mechanism of reaction initiation and light emission of the ctenophore family was largely unknown until our recent QM/MM studies on berovin, in which we proposed a catalytic mechanism predicting that Asp-158–Arg-41–Tyr-204 triad, equivalent to the His-175–Tyr-190–Trp-179 triad (obelin numbering) in the cnidarian family, could shuttle a proton from the 2-hydroperoxy group of coelenterazine to bulk solvent (25). The QM/MM studies on the coelenterazine bound mnemiopsin1 suggest a break of the N_4–C_3 bond and decarboxylation of coelenterazine (30) triggers the bioluminescence reaction in the ctenophore family (Fig. 5).

Studies on the bioluminescence mechanism of cnidarian photoproteins show that some intermediates are involved in the oxidative decarboxylation of coelenterazine (8). They suggest that after the release of CO_2, the primary excited product was an amide anion, which would be expected to be rapidly protonated before it has a chance for radiative emission (8). There are a number of proton sources for this reaction in the binding cavity of mnemiopsin1. One candidate is Tyr-138, which is already hydrogen-bonded to the N_1 of peroxycoelenterazine, assuming that it does not shift its position when the excited amide anion is formed (8). Although the position of this amino acid in structures of aequorin and obelin is almost identical, its mutation is associated with different outcomes for each protein, probably because of slight differences in the mechanism. For instance, Y132F mutation resulted in the loss of aequorin bioluminescence activity, whereas mutation of its corresponding residue in obelin (Tyr-138) retains 60% of its activity. Under the proposed mechanism, it was assumed that the proton transfer was from Tyr-138 to a dioxetanone intermediate. If this is the case, we would expect the Y138F mutant to be similarly inactive (16). In addition, the crystal structure of obelin after the bioluminescence discharge showed that Tyr-138 is replaced by a water molecule. Thus, it was proposed that the critical function of this water molecule is to catalyze the decarboxylation reaction by protonating the dioxetanone anion (34). This was supported by the structure determination of the Y138F mutant of obelin in coelenterazine and coelenteramide-bound states by Natashin *et al.* (16). In the native obelin structure, the coelenterazine N_1 atom is located at a distance of 2.7 Å from the hydroxyl group of Tyr-138. This residue in turn interacts with the nitrogen atom of His-64 via a water molecule. However, the crystallographic results of the Y138F mutant revealed the lack of the aforementioned water molecule and subsequent hydrogen bond network around the N_1 of 2-hydroperoxycoelenterazine. Additionally, the investigation into the hydrogen-bonding network of the coelenteramide-bound Y138F mutant indicates a water molecule within the cavity that connects N_1 of coelenteramide to His-64 (16). These results are consistent with the hypothesis that proton transfer from His-64 to the nitrogen atom of coelenteramide occurs via a water molecule.

To investigate whether a similar mechanism could occur in the ctenophore family, we examined the coelenteramide-bound mnemiopsin1 using QM/MM calculations. The most remarkable finding from these results is the presence a water molecule as a hydrogen bond donor near the amide N of coelenteramide that hydrogen bonds to Tyr-131. Similar to the cnidarian family, a possible function from this water molecule is to catalyze the decarboxylation reaction by protonating the dioxetanone anion, which then yields the neutral coelenteramide as the primary excited product in bioluminescence (Fig. 6). Additional support for this suggestion is found in the mutation study of the Tyr-131 in mnemiopsin1. Structural alignment shows that Tyr-131 of mnemiopsin1 is equivalent to Tyr-132 and Tyr-138 in aequorin and obelin, respectively. The replacement of

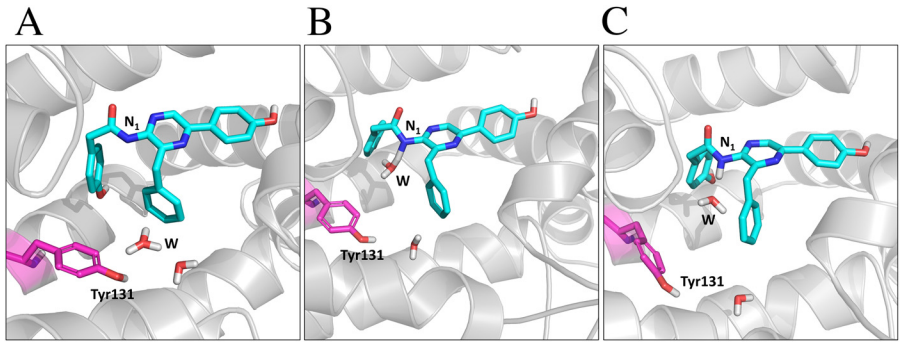

Figure 6. Close-up views of the last snapshot of coelenteramide binding. *A*, before QM/MM initiation. *B*, during QM/MM calculation. *C*, after QM/MM calculation.

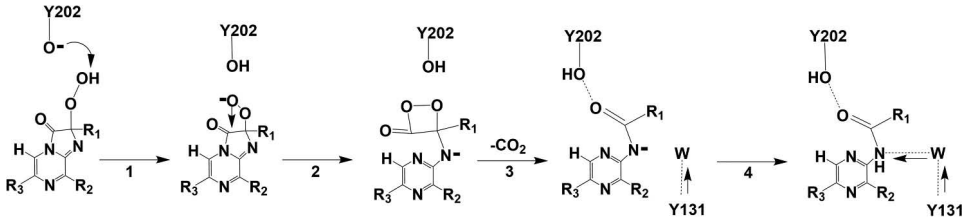

SCHEME 1. **Suggested mechanism for the light emission in the ctenophore family.**

Tyr-131 to Phe leads to the loss of activity compared with the WT protein, which could be related to suppression of protonation of the dioxetanone anion through a water molecule (25). Finally, it has been proposed that the triggering step in bioluminescence of the ctenophore photoproteins involves transfer of a proton from the 2-hydroperoxy group of coelenterazine to Tyr-202 and deprotonation of hydroperoxide (Scheme 1, *step 1*), followed by formation of the dioxetanone anion (Scheme 1, *step 2*). Our computational studies showed that dioxetanone anion intermediate is unstable in this step, resulting in the release of CO_2 (Scheme 1, *step 3*). The structural investigations showed that there is a water molecule near amide N_1 atom of coelenteramide. In addition, the protonation of the anion from the water molecule occurs and produces the neutral coelenteramide as the primary excited product in the bioluminescence (Scheme 1, *step 4*).

In conclusion, we have determined the three-dimensional crystal structure of apo-mnemiopsin1 from the ctenophore family in the cadmium-loaded state. The structure revealed that mnemiopsin1 retains the structural fold characteristic of cnidarian photoproteins despite there being low sequence identity. Our recent QM/MM study on berovin suggested that the Asp-158–Arg-41–Tyr-204 triad is equivalent to the His-175–Tyr-190–Trp-179 triad in obelin and could play an important role in triggering bioluminescence. In the present study, a QM/MM study on mnemiopsin1 suggested that an Asp-156–Arg-39–Tyr-202 triad creates a hydrogen-bonded network so that the proton is transferred from the 2-hydroperoxy group of coelenterazine to bulk solvent. A QM/MM study on the coelenteramide-bound mnemiopsin1 indicated the presence of a water molecule in close distance to the amide N atom of coelenteramide. Thus, it appears that despite the low sequence identity between two these families, the function of the water molecule is to catalyze the decarboxylation reaction by protonating the dioxetanone anion, as previously suggested for the cnidarian family. Confirmation of this mechanism awaits the determination of a 3D atomic structure of a ctenophore in its holo-form state.

Experimental procedures

Bacterial strain and growth condition

Mnemiopsin1-encoding gene (GenBank™ accession no. GQ231544) (26) was cloned into pProEX-HTb between the EheI and HindIII restriction sites. Transformed *Escherichia coli* BL21(DE3)Star cells (Novogen) were grown in Luria-Bertani (LB) medium containing ampicillin to an A_{600} of ~0.6, and protein expression was induced by the addition of isopropyl-β-D-thiogalactoside (final concentration, 0.5 mM). The cells were cultured at 27 °C for 5 h before being harvested. The cells were centrifuged at 3,000 × *g* for 30 min at 4 °C. Cell pellets were stored at −20 °C.

Purification of mnemiopsin1

Bacteria pellets were resuspended in 500 mM NaCl, 10 mM imidazole, 100 mM Tris, pH 7.5, and were lysed using an EmulsiFlex-C_5 homogenizer (Avestin, Ottawa, Canada) with insoluble cell debris being removed by centrifugation at 38,000 × *g* at 4 °C for 30 min. The soluble fraction was applied to a 5-ml HiTrap HP Sepharose column (GE Healthcare) equilibrated with buffer A (500 mM NaCl, 100 mM Tris, pH 7.5). The column was washed with buffer A for 100 ml. Bound proteins were eluted in a 100 ml of 0–100% gradient of buffer A to B (500 mM NaCl, 100 mM Tris, 1 M imidazole, pH 7.5).

The buffer was exchanged with 25 mM Hepes, pH 7.7, 100 mM NaCl, 1 mM TCEP using a HiPrep 26/10 desalting column (GE Healthcare) and then concentrated to 4 ml using 10-kDa molecular mass cutoff Ultra-4 centrifugal filters (Merck Millipore). TEV protease was added in a (w/w) ratio of 1_{TEV}:$100_{Mnemiopsin1}$ and then incubated at 4 °C overnight. The protein solution was passed down a second HiTrap HP Sepharose column (pre-equilibrated with buffer A) to remove the cleaved hexahistidine tag from uncleaved protein, as well as the TEV

protease. Cleaved mnemiopsin1 protein appeared in the flow-through. To ensure the EF-hands of mnemiopsin1 were fully occupied with cadmium ions, concentrated mnemiopsin1 was dialyzed overnight into Cd^{2+} charging buffer composed of 20 mM Tris, pH 8.0, 150 mM NaCl, and 5 mM $CdCl_2$. The protein sample was then applied to a High-load Superdex 75 16/600 gel filtration (GE Healthcare) column, pre-equilibrated with 10 mM Tris, pH 7.5, and 20 mM NaCl. Mnemiopsin1 eluted at a molecular mass corresponding to a monomeric species of 24,500 Da. Fractions were collected and analyzed by SDS-PAGE. Fractions containing mnemiopsin1 were pooled and concentrated to the desired protein concentration.

Crystallization

Initial crystallization trials were carried out using the PEG suite (Qiagen) in 96-well sitting drop vapor diffusion plates (Rigaku). Screens were made by adding 30 μl of crystallant to the well and then adding 0.2 μl of crystallant to 0.2 μl of protein (at 20.5 mg/ml) to form the sitting drops, using a Gryphon robot (Art Robbins Instruments). A single crystal measuring 150 μm × 150 μm × 100 μm was observed after 11 months at 21 °C using the crystallant 20% PEG 3350 and 200 mM KCN. The crystal grew as a hexagonal bipyramid that fluoresced under UV light when viewed using a Rigaku Minstrel DT imager. The crystal was flash-cooled prior to data collection by passing it briefly through Paratone-N (Hampton Research) before being plunged directly into liquid nitrogen.

X-ray diffraction, structure determination, and refinement

The crystal formed in the hexagonal space group $P6_5$, with unit cell dimensions $a = b = 72.61$ Å, $c = 81.43$ Å. One molecule in the asymmetric unit gave a predicted Matthews coefficient of 2.68 $Å^3$ Da^{-1} and a corresponding solvent content of 54.1%. All diffraction data were collected at the Australian Synchrotron, Beamline 3BM2 at 100 K using the program Blue-Ice (35). The data were integrated using XDS (36) and scaled using SCALA (37). Initial phase information was generated by the molecular replacement method with berovin (PDB code 5BPJ) as the search model using the program MolRep (38). ARP/wARP (39) was used to automatically build an initial model. Successive rounds of model building using COOT (40) and refinement using the program PHENIX (41) were carried out using data between 36.30 and 2.15 Å resolution. Residues 196–206 were not visible in the electron density and thus were not modeled. The final model has a R_{factor} of 16.1% and R_{free} of 20.3%. Secondary structural elements were calculated using DSSP (42). A summary of the crystallographic data collection and the refinement statistics is given in Table 2. Structure figures were generated using PyMOL (43).

Table 2
Crystallography statistics

Data collection	
Space group	$P6_5$
Cell dimensions (Å)	
a	72.61
b	72.61
c	81.43
Resolution (Å)[a]	40.71–2.15 (2.22–2.15)
Completeness (%)	99.5 (94.5)
$I/\sigma I$	16.3 (3.9)
R_{merge} (%)	11.7 (61.6)
$R_{p.i.m.}$ (%)	2.9 (16.8)
Redundancy	16.9 (14.3)
Refinement	
Resolution (Å)	34.18–2.15
No. of reflections	25,973
R_{work} (%)/R_{free} (%)[b]	16.1/20.3
Non-hydrogen atoms[c]	1784
Protein	1658 (37.78)
Water	118 (39.48)
Ligands	
Cadmium ions	4 (29.98)
Thiocyanate ions	3 (45/58)
Nickel ions	1 (36.59)
RMSD	
Bond lengths (Å)	0.012
Bond angles (°)	1.19
Ramachandran plot	
Most favored and allowed region (%)	99.48

[a] The values in parentheses represent the highest resolution shell.
[b] R_{free} is based on 5% of the total reflections excluded from refinement.
[c] The values in parentheses represent the average B factor in $Å^2$.

Initial structure preparation and docking studies

The crystal structure of mnemiopsin1 was used as input for the computational studies. Using the I-Tasser server (44–46), missing residues 196–206 were added (I-TASSER threads the protein sequence through the PDB structure library and searches for the possible alignments using *ab initio* modeling for unaligned regions). The resultant model was refined by MD simulation using the AMBER12 software package (47) with ff99SB force field (48). The binding orientation of coelenterazine and coelenteramide were determined using the docking program AutoDock (29–33). The structures apo-aequorin and holo-aequorin show a displacement in the C-terminal helix (23). This movement of the C-terminal helix in apo-mnemiopsin1 was also carried out, thus allowing the coelenterazine to penetrate into the cavity.

Molecular dynamics simulation

The final best-ranked complexes were minimized and used for MD simulations. The AMBER12 package (47) was used for preparation of two complexes. The Antechamber module was applied to calculate the AM1-BCC charges of coelenterazine and coelenteramide. Then ff99SB (48, 49) and GAFF force fields (50) were used to model the complexes with the addition of sodium ions for neutralizing the systems. The resulting complexes were solvated with TIP3P water molecules in a truncated octahedron periodic box with an 8 Å radius buffer zone of water molecules around the complexes. The systems were neutralized by adding the corresponding number of counterions (Na^+) using the LEaP module. Then the systems were energy minimized for 50,000 cycles, using the steepest descent algorithm together with the conjugate gradient method to remove any bad contacts between atoms. The minimized systems were first gradually heated to 300 K over 100 ps using a Langevin thermostat (51) in a constant condition (NVT). The systems were equilibrated for 100 ps at constant pressure (1 atm) with a 2-fs time step to adjust the periodic box size in a constant condition (NPT). Finally, 30 ns unrestrained production simulation was conducted for each system using an integration time step of 2.0 fs. During the production stage, after every 500 time steps, coordinates were saved and used for energy and structure calculation. The MD simulations were done employing periodic

boundary conditions with a 10 Å cutoff for nonbonded interactions, and long-range electrostatics interactions were carried out adhering to the particle mesh Ewald method (52). The SHAKE algorithm (53) was used to fix all covalent bonds involving hydrogen atoms.

QM/MM simulations

The two QM/MM simulations were performed using the AMBER12 program (47). The QM/MM simulations were carried out using the PM6 method (54–56) implemented in AMBER12. In the QM/MM simulations, final complex configurations resulting from the classical MD simulations were used as the initial structure. In the first QM/MM, QM part consisted of the coelenterazine and side chain of Tyr-202 so that tyrosine residue was manually deprotonated to form a tyrosinate anion. The QM region of the second QM/MM includes the coelenteramide and H_3O^+. The rest of the protein, water molecules and (Na^+, Cl^-) ions were considered as the MM region. The MM part was defined by AMBER ff99SB force fields (48, 49).

Author contributions—M. M., M. A. G., A. M., Z. P., and M. T. data curation; M. M., M. A. G., A. M., Z. P., M. T., and R. H. S. formal analysis; M. M., M. A. G., A. M., M. T., H. N.-M., and R. H. S. validation; M. M., M. A. G., M. T., H. N.-M., and R. H. S. investigation; M. M., M. A. G., H. N.-M., and R. H. S. visualization; M. M., M. A. G., A. M., Z. P., M. T., and R. H. S. methodology; M. M. and M. A. G. writing-original draft; M. M., M. A. G., A. M., Z. P., M. T., H. N.-M., R. H. S., and M. W. P. writing-review and editing; M. A. G., A. M., Z. P., M. T., H. N.-M., R. H. S., and M. W. P. supervision; M. A. G., H. N.-M., R. H. S., and M. W. P. project administration; H. N.-M. and R. H. S. conceptualization; H. N.-M., R. H. S., and M. W. P. resources; R. H. S. and M. W. P. funding acquisition.

Acknowledgments—We thank the MX2 Beamline staff at the Australian Synchrotron for their expert help.

References

1. Chalfie, M., Tu, Y., Euskirchen, G., Ward, W. W., and Prasher, D. C. (1994) Green fluorescent protein as a marker for gene expression. *Science* **263,** 802–805 CrossRef Medline
2. Ward, W. W., Swiatek, G. C., and Gonzalez, D. G. (2000) Green fluorescent protein in biotechnology education. *Methods Enzymol.* **305,** 672–680 CrossRef Medline
3. Contag, C. H., and Bachmann, M. H. (2002) Advances in *in vivo* bioluminescence imaging of gene expression. *Annu. Rev. Biomed. Enging.* **4,** 235–260 CrossRefMedline
4. González, J. E., and Negulescu, P. A. (1998) Intracellular detection assays for high-throughput screening. *Curr. Opin. Biotech.* **9,** 624–631 CrossRef Medline
5. Kain, S. R. (1999) Green fluorescent protein (GFP): applications in cell-based assays for drug discovery. *Drug Discov. Today* **4,** 304–312 CrossRef Medline
6. DiPilato, L. M., Cheng, X., and Zhang, J. (2004) Fluorescent indicators of cAMP and Epac activation reveal differential dynamics of cAMP signaling within discrete subcellular compartments. *Proc. Natl. Acad. Sci. U.S.A.* **101,** 16513–16518 CrossRef Medline
7. Shimomura, O., and Johnson, F. H. (1972) Structure of the light-emitting moiety of aequorin. *Biochemistry* **11,** 1602–1608 CrossRef Medline
8. Vysotski, E. S., and Lee, J. (2004) Ca^{2+}-regulated photoproteins: structural insight into the bioluminescence mechanism. *Acc. Chem. Res.* **37,** 405–415 CrossRef Medline
9. Shimomura, O. (2012) *Bioluminescence: Chemical Principles and Methods*, World Scientific, Singapore
10. Deng, L., Vysotski, E. S., Markova, S. V., Liu, Z. J., Lee, J., Rose, J., and Wang, B. C. (2005) All three Ca^{2+}-binding loops of photoproteins bind calcium ions: the crystal structures of calcium-loaded apo-aequorin and apo-obelin. *Protein Sci.* **14,** 663–675 CrossRef Medline
11. Head, J. F., Inouye, S., Teranishi, K., and Shimomura, O. (2000) The crystal structure of the photoprotein aequorin at 2.3 Å resolution. *Nature* **405,** 372–376 CrossRef Medline
12. Liu, Z.-J., Vysotski, E. S., Deng, L., Lee, J., Rose, J., and Wang, B.-C. (2003) Atomic resolution structure of obelin: soaking with calcium enhances electron density of the second oxygen atom substituted at the C_2-position of coelenterazine. *Biochem. Biophys. Res. Commun.* **311,** 433–439 CrossRef Medline
13. Titushin, M. S., Feng, Y., Stepanyuk, G. A., Li, Y., Markova, S. V., Golz, S., Wang, B.-C., Lee, J., Wang, J., Vysotski, E. S., and Liu, Z.-J. (2010) NMR-derived topology of a GFP-photoprotein energy transfer complex. *J. Biol. Chem.* **285,** 40891–40900 CrossRef Medline
14. Deng, L., Vysotski, E. S., Liu, Z.-J., Markova, S. V., Malikova, N. P., Lee, J., Rose, J., and Wang, B.-C. (2001) Structural basis for the emission of violet bioluminescence from a W92F obelin mutant. *FEBS Lett.* **506,** 281–285 CrossRef Medline
15. Vysotski, E. S., Liu, Z.-J., Markova, S. V., Blinks, J. R., Deng, L., Frank, L. A., Herko, M., Malikova, N. P., Rose, J. P., Wang, B. C., and Lee, J. (2003) Violet bioluminescence and fast kinetics from W92F obelin: structure-based proposals for the bioluminescence triggering and the identification of the emitting species. *Biochemistry* **42,** 6013–6024 CrossRef Medline
16. Natashin, P. V., Ding, W., Eremeeva, E. V., Markova, S. V., Lee, J., Vysotski, E. S., and Liu, Z.-J. (2014) Structures of the Ca^{2+}-regulated photoprotein obelin Y138F mutant before and after bioluminescence support the catalytic function of a water molecule in the reaction. *Acta Crystallogr. D Biol. Crystallogr.* **70,** 720–732 CrossRef Medline
17. Natashin, P. V., Markova, S. V., Lee, J., Vysotski, E. S., and Liu, Z. J. (2014) Crystal structures of the F88Y obelin mutant before and after bioluminescence provide molecular insight into spectral tuning among hydromedusan photoproteins. *FEBS J.* **281,** 1432–1445 CrossRef Medline
18. Stepanyuk, G. A., Liu, Z.-J., Burakova, L. P., Lee, J., Rose, J., Vysotski, E. S., and Wang, B.-C. (2013) Spatial structure of the novel light-sensitive photoprotein berovin from the ctenophore Beroe abyssicola in the Ca^{2+}-loaded apoprotein conformation state. *Biochim. Biophys. Acta* **1834,** 2139–2146 CrossRef Medline
19. Burakova, L. P., Natashin, P. V., Malikova, N. P., Niu, F., Pu, M., Vysotski, E. S., and Liu, Z.-J. (2016) All Ca^{2+}-binding loops of light-sensitive ctenophore photoprotein berovin bind magnesium ions: the spatial structure of Mg^{2+}-loaded apo-berovin. *J. Photochem. Photobiol. B* **154,** 57–66 CrossRef Medline
20. Mahdavi, A., Sajedi, R. H., Hosseinkhani, S., Taghdir, M., and Sariri, R. (2013) Site-directed mutagenesis of photoprotein mnemiopsin: implication of some conserved residues in bioluminescence properties. *Photochem. Photobiol. Sci.* **12,** 467–478 CrossRef Medline
21. Mahdavi, A., Sajedi, R. H., Hosseinkhani, S., and Taghdir, M. (2015) Hyperactive Arg39Lys mutated mnemiopsin: implication of positively charged residue in chromophore binding cavity. *Photochem. Photobiol. Sci.* **14,** 792–800 CrossRef Medline
22. Hakiminia, F., Molakarimi, M., Khalifeh, K., Jahani, Z., Sajedi, R. H., and Ranjbar, B. (2016) Adjustment of local conformational flexibility and accessible surface area alterations of serine 128 and valine 183 in mnemiopsin. *J. Mol. Struct.* **1117,** 287–292 CrossRef
23. Burakova, L. P., Stepanyuk, G. A., Eremeeva, E. V., and Vysotski, E. S. (2016) Role of certain amino acid residues of the coelenterazine-binding cavity in bioluminescence of light-sensitive Ca^{2+}-regulated photoprotein berovin. *Photochem. Photobiol. Sci.* **15,** 691–704 CrossRef Medline
24. Pashandi, Z., Molakarimi, M., Sajedi, R. H., Taghdir, M., and Naderi-Manesh, H. (2016) Light induced structural changes of the photoprotein mnemiopsin: characterization and contribution in photoinactivation. *J. Photochem. Photobiol. B* **165,** 133–140 CrossRef Medline
25. Molakarimi, M., Mohseni, A., Taghdir, M., Pashandi, Z., Gorman, M. A., Parker, M. W., Naderi-Manesh, H., and Sajedi, R. H. (2017) QM/MM

simulations provide insight into the mechanism of bioluminescence triggering in ctenophore photoproteins. *PLoS One* **12,** e0182317 CrossRef Medline
26. Aghamaali, M. R., Jafarian, V., Sariri, R., Molakarimi, M., Rasti, B., Taghdir, M., Sajedi, R. H., and Hosseinkhani, S. (2011) Cloning, sequencing, expression and structural investigation of mnemiopsin from *Mnemiopsis leidyi*: an attempt toward understanding Ca^{2+}-regulated photoproteins. *Protein J.* **30,** 566–574 CrossRef Medline
27. Pashandi, Z., Molakarimi, M., Mohseni, A., Sajedi, R. H., Taghdir, M., and Naderi-Manesh, H. (2017) Photoinactivation related dynamics of ctenophore photoproteins: insights from molecular dynamics simulation under electric-field. *Biochem. Biophys. Res. Commun.* **490,** 265–270 CrossRef Medline
28. Cates, M. S., Berry, M. B., Ho, E. L., Li, Q., Potter, J. D., and Phillips, G. N., Jr. (1999) Metal-ion affinity and specificity in EF-hand proteins: coordination geometry and domain plasticity in parvalbumin. *Structure* **7,** 1269–1278 CrossRef Medline
29. Goodsell, D. S., and Olson, A. J. (1990) Automated docking of substrates to proteins by simulated annealing. *Proteins* **8,** 195–202 CrossRef Medline
30. Morris, G. M., Goodsell, D. S., Halliday, R. S., Huey, R., Hart, W. E., Belew, R. K., and Olson, A. J. (1998) Automated docking using a Lamarckian genetic algorithm and an empirical binding free energy function. *J. Comput. Chem.* **19,** 1639–1662 CrossRef
31. Morris, G. M., Huey, R., Lindstrom, W., Sanner, M. F., Belew, R. K., Goodsell, D. S., and Olson, A. J. (2009) AutoDock4 and AutoDockTools4: automated docking with selective receptor flexibility. *J. Comput. Chem.* **30,** 2785–2791 CrossRef Medline
32. Huey, R., Morris, G. M., Olson, A. J., and Goodsell, D. S. (2007) A semiempirical free energy force field with charge-based desolvation. *J. Comput. Chem.* **28,** 1145–1152 CrossRef Medline
33. Ravindranath, P. A., Forli, S., Goodsell, D. S., Olson, A. J., and Sanner, M. F. (2015) AutoDockFR: advances in protein-ligand docking with explicitly specified binding site flexibility. *PLoS Comput. Biol.* **11,** e1004586 CrossRef Medline
34. Liu, Z.-J., Stepanyuk, G. A., Vysotski, E. S., Lee, J., Markova, S. V., Malikova, N. P., and Wang, B.-C. (2006) Crystal structure of obelin after Ca^{2+}-triggered bioluminescence suggests neutral coelenteramide as the primary excited state. *Proc. Natl. Acad. Sci. U.S.A.* **103,** 2570–2575 CrossRef Medline
35. McPhillips, T. M., McPhillips, S. E., Chiu, H.-J., Cohen, A. E., Deacon, A. M., Ellis, P. J., Garman, E., Gonzalez, A., Sauter, N. K., Phizackerley, R. P., Soltis, S. M., and Kuhn, P. (2002) Blu-Ice and the Distributed Control System: software for data acquisition and instrument control at macromolecular crystallography beamlines. *J. Synchrotron Radiat.* **9,** 401–406 CrossRef Medline
36. Kabsch, W. (2006) Integration, scaling, space-group assignment and post refinement. In *International Tables for Crystallography Volume F: Crystallography of Biological Macromolecules*, pp. 218–225, Springer-Verlag, New York Inc., New York
37. Evans, P. (2006) Scaling and assessment of data quality. *Acta Crystallogr. D Biol. Crystallogr.* **62,** 72–82 CrossRef Medline
38. Vagin, A., and Teplyakov, A. (2010) Molecular replacement with MOLREP. *Acta Crystallogr. D Biol. Crystallogr.* **66,** 22–25 CrossRef Medline
39. Langer, G., Cohen, S. X., Lamzin, V. S., and Perrakis, A. (2008) Automated macromolecular model building for X-ray crystallography using ARP/wARP version 7. *Nat. Protoc.* **3,** 1171–1179 CrossRef Medline
40. Emsley, P., and Cowtan, K. (2004) Coot: model-building tools for molecular graphics. *Acta Crystallogr. D Biol. Crystallogr.* **60,** 2126–2132 CrossRef Medline
41. Adams, P. D., Grosse-Kunstleve, R. W., Hung, L.-W., Ioerger, T. R., McCoy, A. J., Moriarty, N. W., Read, R. J., Sacchettini, J. C., Sauter, N. K., and Terwilliger, T. C. (2002) PHENIX: building new software for automated crystallographic structure determination. *Acta Crystallogr. D Biol. Crystallogr* **58,** 1948–1954 CrossRef Medline
42. Kabsch, W., and Sander, C. (1984) On the use of sequence homologies to predict protein structure: identical pentapeptides can have completely different conformations. *Proc. Natl. Acad. Sci. U.S.A.* **81,** 1075–1078 CrossRef Medline
43. DeLano, W. L. (2002) *The PyMOL Molecular Graphics System*, Schroedinger, LLC, New York
44. Zhang, Y. (2008) I-TASSER server for protein 3D structure prediction. *BMC Bioinform.* **9,** 40 CrossRef
45. Roy, A., Kucukural, A., and Zhang, Y. (2010) I-TASSER: a unified platform for automated protein structure and function prediction. *Nat. Protoc.* **5,** 725–738 CrossRef Medline
46. Yang, J., Yan, R., Roy, A., Xu, D., Poisson, J., and Zhang, Y. (2015) The I-TASSER Suite: protein structure and function prediction. *Nat. Methods* **12,** 7–8 CrossRef Medline
47. Case, D. A., Darden, T. A., Cheatham, T. E., III, Simmerling, C. L., Wang, J., Duke, R. E., Luo, R., Walker, R. C., Zhang, W., Merz, K. M., Roberts, B., Hayik, S., Roitberg, A., Seabra, G., Swails, J., *et al.* (2012) *Amber 12*, University of California: San Francisco, CA
48. Lindorff-Larsen, K., Piana, S., Palmo, K., Maragakis, P., Klepeis, J. L., Dror, R. O., and Shaw, D. E. (2010) Improved side-chain torsion potentials for the Amber ff99SB protein force field. *Proteins* **78,** 1950–1958 Medline
49. Hornak, V., Abel, R., Okur, A., Strockbine, B., Roitberg, A., and Simmerling, C. (2006) Comparison of multiple Amber force fields and development of improved protein backbone parameters. *Proteins* **65,** 712–725 CrossRef Medline
50. Wang, J., Wolf, R. M., Caldwell, J. W., Kollman, P. A., and Case, D. A. (2004) Development and testing of a general amber force field. *J. Computat. Chem.* **25,** 1157–1174 CrossRef
51. Pastor, R. W., Brooks, B. R., and Szabo, A. (1988) An analysis of the accuracy of Langevin and molecular dynamics algorithms. *Mol. Physics* **65,** 1409–1419 CrossRef
52. Gilson, M. K., Sharp, K. A., and Honig, B. H. (1988) Calculating the electrostatic potential of molecules in solution: method and error assessment. *J. Comput. Chem.* **9,** 327–335 CrossRef
53. Ryckaert, J.-P., Ciccotti, G., and Berendsen, H. J. (1977) Numerical integration of the cartesian equations of motion of a system with constraints: molecular dynamics of *n*-alkanes. *J. Comput. Phys.* **23,** 327–341 CrossRef
54. Stewart, J. J. (2007) Optimization of parameters for semiempirical methods V: modification of NDDO approximations and application to 70 elements. *J. Mol. Model.* **13,** 1173–1213 CrossRef Medline
55. Stewart, J. J. (1989) Optimization of parameters for semiempirical methods II. Applications. *J. Comput. Chem.* **10,** 221–264 CrossRef
56. Stewart, J. J. (2013) Optimization of parameters for semiempirical methods VI: more modifications to the NDDO approximations and re-optimization of parameters. *J. Mol. Model.* **19,** 1–32 CrossRef Medline